

# Fluorescence and laser properties of Nd-doped $(\text{Ca}_{0.5}\text{Sr}_{0.5})_{10}(\text{PO}_4)_6\text{F}_2$ ceramics

HIROAKI FURUSE,<sup>1,\*</sup>  KAZUYA TAKIMOTO,<sup>1,2</sup> SANAE KOIZUMI,<sup>1</sup> AND HIROYASU SONE<sup>2</sup>

<sup>1</sup>National Institute for Materials Science, 1-2-1 Sengen, Tsukuba, Ibaraki, Japan

<sup>2</sup>Kitami Institute of Technology, 165 Koencho, Kitami, Hokkaido, Japan

\*FURUSE.Hiroaki@nims.go.jp

**Abstract:** Transparent ceramics of Nd<sup>3+</sup>-doped  $(\text{Ca}_{0.5}\text{Sr}_{0.5})_{10}(\text{PO}_4)_6\text{F}_2$  (CS-FAP), a solid solution of hexagonal fluorapatite  $\text{Ca}_{10}(\text{PO}_4)_6\text{F}_2$  (C-FAP) and  $\text{Sr}_{10}(\text{PO}_4)_6\text{F}_2$  (S-FAP), was successfully fabricated. Laser oscillation from Nd:CS-FAP was demonstrated for the first time. The ceramics consisted of fine grains with an average grain size of approximately 100 nm. Despite a non-cubic crystal structure, light scattering due to birefringence was small, and the total loss coefficient near 1  $\mu\text{m}$  was approximately  $0.5\text{ cm}^{-1}$ . The full width at half maximum (FWHM) of the fluorescence spectra was about 3.5 nm ( $31\text{ cm}^{-1}$ ) at 1  $\mu\text{m}$  and 6.4 nm ( $36\text{ cm}^{-1}$ ) at 1.3  $\mu\text{m}$ , respectively. They were substantially broader than those of C-FAP and S-FAP (both approximately 1 nm), resulting from lattice distortion due to solid solution formation. The fluorescence peak wavelengths and laser oscillation wavelengths (1061 nm and 1333 nm) were intermediate between those of C-FAP and S-FAP. The Ca to Sr ratio can be controlled, providing compositional design flexibility and the potential of CS-FAP ceramics as novel ultrashort-pulse laser materials.

© 2026 Optica Publishing Group under the terms of the [Optica Open Access Publishing Agreement](#)

## 1. Introduction

Ceramic laser media are regarded as promising candidates for high pulse energy and high repetition rate laser applications, owing to their thermal conductivity being comparable to that of single crystals, the feasibility of fabricating large-scale and bonding materials, and superior optical homogeneity [1–4]. However, ceramic sintered bodies are more likely to exhibit residual pores, secondary phases, and grain boundary scattering, all of which can act as optical scattering sources and limit the realization of optical properties required for laser applications [5].

It is crucial to minimize optical loss sources in ceramics for laser applications, as they induce an exponential decrease in the in-line transmittance of the ceramics, which is described as follows:

$$T = (1 - R)^2 \exp[-(\alpha + \delta_p + \delta_{s,p} + \delta_g \cdots)L], \quad (1)$$

where  $T$  is the in-line transmittance,  $R$  is the Fresnel reflection,  $\alpha$ ,  $\delta_p$ ,  $\delta_{s,p}$ , and  $\delta_g$  are the loss coefficients due to absorption, residual porosity, secondary phases, and grain boundaries, respectively, and  $L$  is the thickness of the material. In general, a total loss coefficient of  $< 0.01\text{ cm}^{-1}$  is required to achieve laser-grade quality. Consequently, attaining high optical quality in ceramic laser media requires rigorous control of microstructural features that contribute to scattering and absorption losses. While various crystal structures, including non-cubic structures, can be selected for single-crystal laser materials, polycrystalline ceramics are subject to grain boundary scattering  $\delta_g$  induced by birefringence. As a result, laser-grade optical quality has typically been limited to materials with cubic crystal structures, such as YAG and cubic sesquioxides, including  $\text{Y}_2\text{O}_3$ ,  $\text{Lu}_2\text{O}_3$ , and  $\text{Sc}_2\text{O}_3$ .

Hexagonal fluorapatite compounds, such as  $\text{Ca}_{10}(\text{PO}_4)_6\text{F}_2$  (FAP or C-FAP) and  $\text{Sr}_{10}(\text{PO}_4)_6\text{F}_2$  (S-FAP), have been used as single-crystal laser media [6–8]. In particular, Yb:S-FAP single crystals exhibit a higher stimulated emission cross-section than that of YAG, making them promising

candidates for high-power laser applications [9,10]. Recently, there has been considerable interest in fabricating these materials using ceramic techniques.

To achieve laser-grade optical quality in non-cubic polycrystalline ceramics, all loss sources in Eq. (1) must be minimized as much as possible. The magnitude of grain boundary scattering  $\delta_g$ , caused by birefringence can be expressed based on Mie scattering theory as follows [11]:

$$\delta_g = \frac{3\pi^2 d \Delta n^2}{2\lambda^2}. \quad (2)$$

where  $\Delta n$  is the refractive index difference,  $d$  is the average grain size composing the ceramics, and  $\lambda$  is the wavelength of light. Previous approaches to reducing the grain boundary scattering coefficient  $\delta_g$  in fluorapatite ceramic laser media include the use of a magnetic field to align the crystal orientation of grains during the forming process prior to sintering. Rare-earth doping enhances the magnetic anisotropy of otherwise diamagnetic apatite powders, thereby enabling crystal orientation in a magnetic field [12]. This alignment reduces refractive index differences,  $\Delta n$ , as demonstrated in previous studies reporting the first laser oscillation [13] and Q-switched operation [14] in non-cubic ceramics. Another approach is to control the grain size  $d$  to approximately 100 nm, which is significantly smaller than the wavelength of light [15–17]. This is achieved by highly controlled powder preparation and sintering techniques. Laser oscillation has been demonstrated using both methods, indicating the potential for further material development in this field.

Recently, the development of transparent Nd-doped CS-FAP:  $(\text{Ca}_x\text{Sr}_{1-x})_{10}(\text{PO}_4)_6\text{F}_2$  ceramics, which are solid solutions composed of Ca and Sr, has been reported [18]. In such mixed-crystal materials, compositional disorder and differences in the ionic radii of the constituent ions reduce site symmetry, resulting in a more inhomogeneous crystal field and significantly broadened absorption and emission bands [19]. Such compositional tuning enables the development of materials with broad emission bands suitable for ultrashort-pulse generation and has been systematically investigated in various rare-earth-doped mixed materials [20–22]. Accordingly, Nd<sup>3+</sup>-doped CS-FAP ceramics have potential applications as novel materials for ultrashort-pulse lasers; however, laser oscillation has not yet been achieved in Nd:CS-FAP. To the best of our knowledge, the only reported laser oscillation in mixed fluorapatite materials was for Yb:CS-FAP single crystal [23,24].

In this study, we fabricated transparent Nd:CS-FAP ceramics via ceramic processing techniques to obtain broadened emission spectra, with the aim of developing new broadband laser materials for ultrashort pulse generation. We evaluated their fluorescence and laser properties and compared the fluorescence properties of CS-FAP ceramics with those of C-FAP and S-FAP to assess the potential of CS-FAP as a broadband laser material.

## 2. Experimental method

### 2.1. Material preparation

C-FAP and S-FAP powders with a nominal Nd<sup>3+</sup> concentration of 1 at.% were initially synthesized following the procedures described in our previous studies, where detailed information on their crystal structure and microstructure can be found [15,17]. Trivalent Nd<sup>3+</sup> ions can substitute for the divalent Ca<sup>2+</sup> or Sr<sup>2+</sup> sites in the apatite lattice, preferentially occupying the Ca(II) or Sr(II) sites (coordination number = 7). However, owing to the difference in valence, this substitution requires charge compensation, which commonly occurs via the incorporation of O<sup>2-</sup> ions or the formation of fluorine vacancies, thereby maintaining overall charge neutrality [9].

These powders were then mixed at a 1:1 molar ratio of Ca to Sr using a ball mill and subsequently dried. This equimolar ratio was selected because the effects of compositional disorder on lattice distortion and spectral broadening are generally most pronounced near equal proportions of the two cations in mixed-crystal systems. The mixed powders were sintered to

produce Nd-doped CS-FAP  $((\text{Ca}_{0.5}\text{Sr}_{0.5})_{10}(\text{PO}_4)_6\text{F}_2)$  transparent ceramics using a spark plasma sintering system (LABOX-315, Sinter Land), which enables sintering under a vacuum with uniaxial pressure. The sintering temperature was 950°C, the holding time was 20 min, and the applied pressure was 80 MPa. After sintering, both surfaces of the ceramics were mirror-polished. The resulting sample had a diameter of 10 mm and a thickness of approximately 0.8 mm.

For material characterization, the in-line transmittance, crystal structure, and microstructure were evaluated using a UV-VIS-NIR spectrometer (UV-3600i Plus, Shimadzu), X-ray diffraction (XRD, RINT-TTR III, Rigaku), and field emission scanning electron microscope (FE-SEM, S-4800, Hitachi).

## 2.2. Emission and laser properties

Fluorescence spectrum measurements and laser oscillation tests at both 1  $\mu\text{m}$  and 1.3  $\mu\text{m}$  were conducted for Nd:CS-FAP ceramics. A fiber-coupled laser diode (LD) with a wavelength of 808 nm was used as the pump source. The fluorescence and lasing spectra were measured using an optical spectrum analyzer (Q8383, Advantest). Figure 1 presents a schematic of the laser test. The configuration for laser oscillation tests was the same as that used in our previous study [25]. The core diameter and maximum output power of the fiber-coupled LD were 105  $\mu\text{m}$  and 60 W, respectively. The fiber output was focused to approximately 105  $\mu\text{m}$  on the Nd:CS-FAP ceramics using a pair of lenses with identical focal lengths. The LD was operated in quasi-continuous wave (QCW) mode with a pulse width of 1 ms and a repetition rate of 10 Hz, to avoid thermal issues in the gain medium. The laser tests were performed using a cavity length of approximately 1 mm formed by a flat dichroic mirror and a flat output coupler, and the average output power was measured using a power meter.

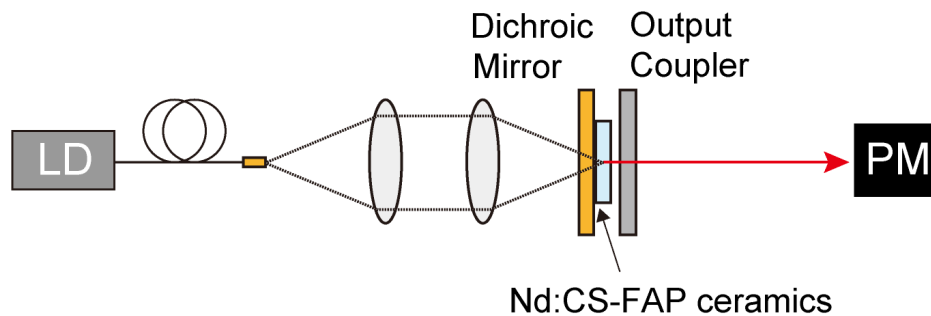


**Fig. 1.** Experimental setup of the laser test for Nd:CS-FAP ceramics.

For the laser tests at 1  $\mu\text{m}$ , the output coupler reflectivity was varied from 70–99% to determine the optimal output coupler reflectivity. For the 1.3  $\mu\text{m}$  wavelength range, a reflectivity of 90% was used.

## 3. Results and discussion

### 3.1. Material characteristics

Figure 2(a) shows a photograph of the sample and in-line transmittance spectrum of Nd:CS-FAP ceramics. The dashed line indicates the theoretical transmittance calculated from the average refractive indices of C-FAP and S-FAP [9,26]. The in-line transmittance at the laser wavelength of 1060 nm was 85.7%, which corresponds to a total loss coefficient of approximately  $0.5\text{ cm}^{-1}$ . The reduction in transmittance at shorter wavelengths was mainly attributed to a small number of residual pores and grain boundary scattering, which cannot be eliminated in

fine polycrystalline ceramics. Laser-grade optical quality (total loss coefficient  $< 0.01 \text{ cm}^{-1}$ ) requires minimizing these loss sources. Achieving this will require further refinement of ceramic processing conditions, including optimization of powder synthesis, high-density compaction, and post-sintering treatments such as hot isostatic pressing (HIP).

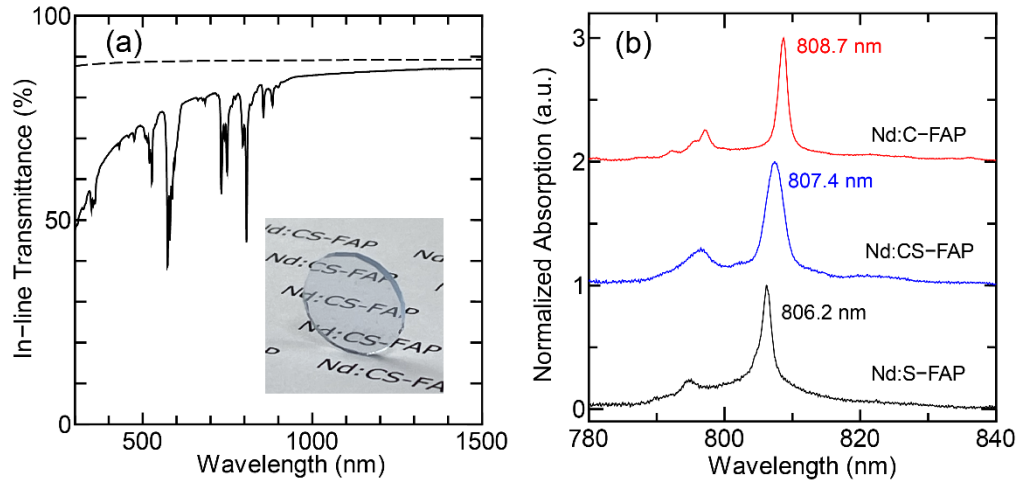
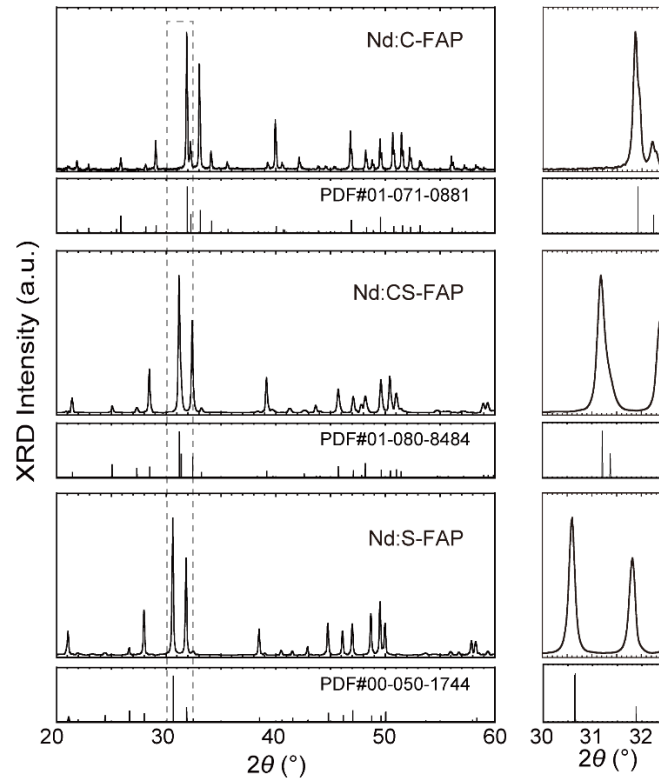


**Fig. 2.** (a) In-line transmittance and (b) absorption intensity of Nd:CS-FAP ceramics.

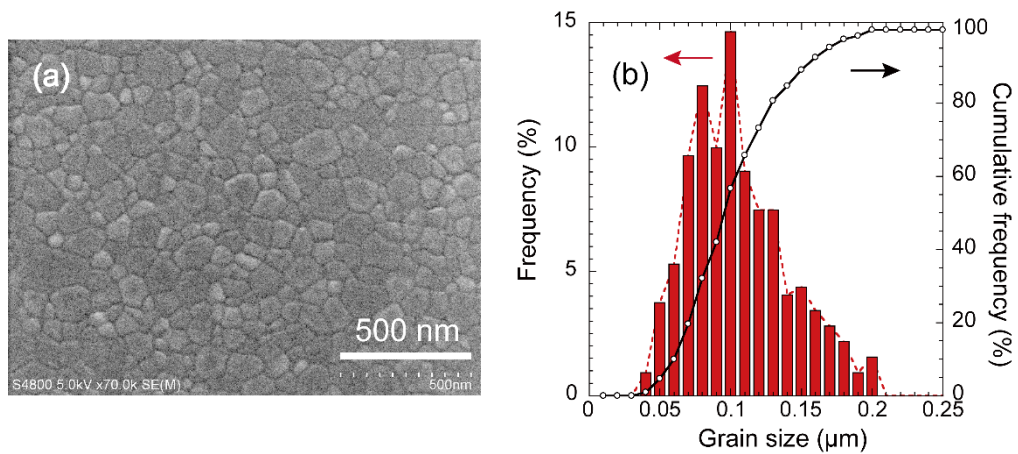
Figure 2(b) shows the normalized absorption spectra around the excitation wavelength. The absorption values were first calculated using the total loss coefficient derived from the in-line transmittance and sample thickness based on Eq. (1). The baseline scattering coefficient was then subtracted to isolate the absorption attributable only to  $\text{Nd}^{3+}$  ions. Each spectrum was subsequently normalized to its maximum value. The absorption peak wavelengths for C-FAP, S-FAP, and CS-FAP were 808.7 nm, 806.2 nm, and 807.4 nm, respectively. Among these compositions, CS-FAP exhibited a much broader absorption band.

Figure 3 shows the XRD patterns of Nd:CS-FAP ceramics, along with those of Nd:C-FAP and Nd:S-FAP for comparison. XRD analysis confirmed that Nd:CS-FAP formed a single-phase apatite structure. Furthermore, the XRD patterns indicate that the ceramics were composed of grains with nearly random orientations. Figure 3 also presents an enlarged view of the peaks between  $30^\circ$  and  $32.5^\circ$ , revealing that the main diffraction peak of Nd:CS-FAP was located between those of C-FAP and S-FAP. These results suggest that Ca and Sr were homogeneously incorporated into the apatite lattice to form a solid solution. The lattice parameters estimated from these XRD peak positions are as follows (in Å): Nd:C-FAP ( $a = 9.38$ ,  $c = 6.89$ ), Nd:CS-FAP ( $a = 9.56$ ,  $c = 7.09$ ), and Nd:S-FAP ( $a = 9.73$ ,  $c = 7.28$ ). The gradual increase in both lattice parameters with increasing Sr content provides further evidence of the formation of a continuous solid solution.

Figure 4(a) shows the microstructure of the polished ceramic surface after thermal etching at  $800^\circ\text{C}$ . The ceramics were dense, with no significant residual pores, secondary phases, or other scattering sources observed. Figure 4(b) shows the grain size distribution evaluated from FE-SEM images. The average grain size was calculated from at least 300 individual grains by determining the equivalent circular diameter under assumption of spherical grains [11]. The grain sizes ranged from approximately 50 to 200 nm, with an average grain size of about 100 nm. This grain size and morphology are comparable to those previously reported for Nd:C-FAP and Nd:S-FAP ceramics [15,17].



**Fig. 3.** XRD peak pattern for Nd:C-FAP, Nd:CS-FAP and Nd:S-FAP ceramics.



**Fig. 4.** (a) FE-SEM image of the polished surface of Nd:CS-FAP ceramics. (b) Grain size distribution of the ceramics, showing an average grain size of approximately 100 nm.

In addition to improving the ceramic processing to enhance optical quality, evaluating optical homogeneity is also important. In future work, we aim to further improve material quality by assessing the transmitted wavefront after polishing and conducting elemental analysis of the microstructure.

### 3.2. Fluorescence and laser properties

Figures 5(a) and (b) show the fluorescence spectra of Nd:CS-FAP in the 1  $\mu\text{m}$  and 1.3  $\mu\text{m}$  wavelength ranges, which correspond to the  $^4F_{3/2} \rightarrow ^4I_{11/2}$  and  $^4F_{3/2} \rightarrow ^4I_{13/2}$  transitions of  $\text{Nd}^{3+}$  ions, respectively. For comparison, the spectra of the Nd:C-FAP and Nd:S-FAP were also included. In the spectra of Nd:CS-FAP, a peak shift and spectral broadening were observed at both wavelengths, attributable to the solid solution effects of Ca and Sr. The FWHM values for C-FAP and S-FAP are approximately 1 nm (corresponding to  $9\text{ cm}^{-1}$  at 1060 nm and  $6\text{ cm}^{-1}$  at 1330 nm), while Nd:CS-FAP exhibited FWHM values of 3.5 nm ( $31\text{ cm}^{-1}$ ) at 1061 nm and 6.4 nm ( $36\text{ cm}^{-1}$ ) at 1330 nm, respectively. These spectral widths correspond to potential pulse durations of 340 fs and 290 fs at 1061 nm and 1330 nm, achievable through mode-locked operation. These results highlight the potential of Nd:CS-FAP as a novel ultrashort-pulse laser material.

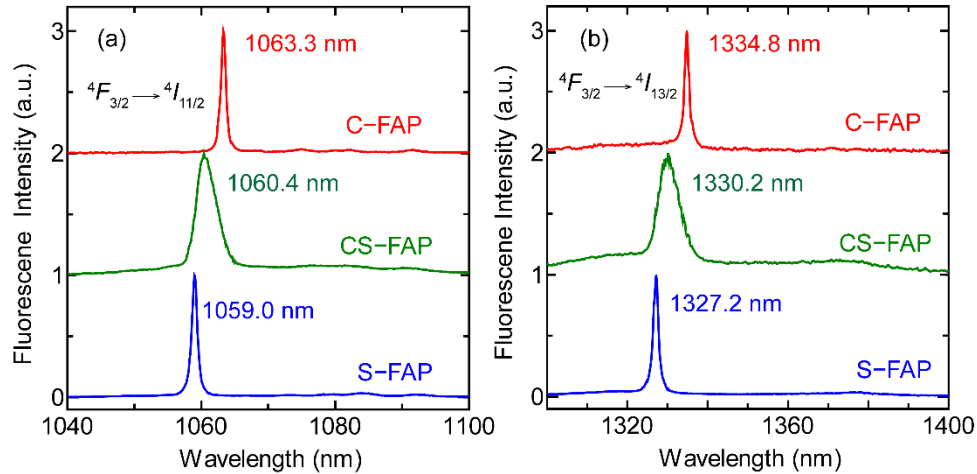


**Fig. 5.** Comparison of the emission properties of Nd:C-FAP, Nd:CS-FAP and Nd:S-FAP for (a) 1  $\mu\text{m}$  and (b) 1.3  $\mu\text{m}$  wavelengths.

Figure 6 shows the temporal decay curves of Nd:CS-FAP ceramics together with those of Nd:C-FAP and Nd:S-FAP. The fluorescence was detected at around 1  $\mu\text{m}$  (corresponding to the  $^4F_{3/2} \rightarrow ^4I_{11/2}$  transition) using a Si photodetector and a 1000 nm long-pass filter. No significant quenching processes were observed for CS-FAP ceramics, and the fluorescence lifetime, determined by single-exponential fitting, was 186  $\mu\text{s}$ . This value lies between the lifetimes of C-FAP (156  $\mu\text{s}$ ) and S-FAP (218  $\mu\text{s}$ ). The trend of an increasing fluorescence lifetime with a higher Sr concentration was also observed in a previous study [18], possibly due to differences in the phonon energies of the C-FAP and S-FAP hosts, which affect the rate of non-radiative transitions.

Figures 7(a) and (b) show the laser properties at wavelengths of 1  $\mu\text{m}$  and 1.3  $\mu\text{m}$ , respectively. Typical lasing spectra are also shown, with oscillation observed at 1061 nm and 1333 nm. The maximum output and slope efficiency of 6.3 mW and 6.1%, respectively, at 1  $\mu\text{m}$  was obtained with an output coupler reflectivity of 90%. The slope efficiency was somewhat lower than the values exceeding 10% reported for Nd:C-FAP and Nd:S-FAP. This reduction may be attributed



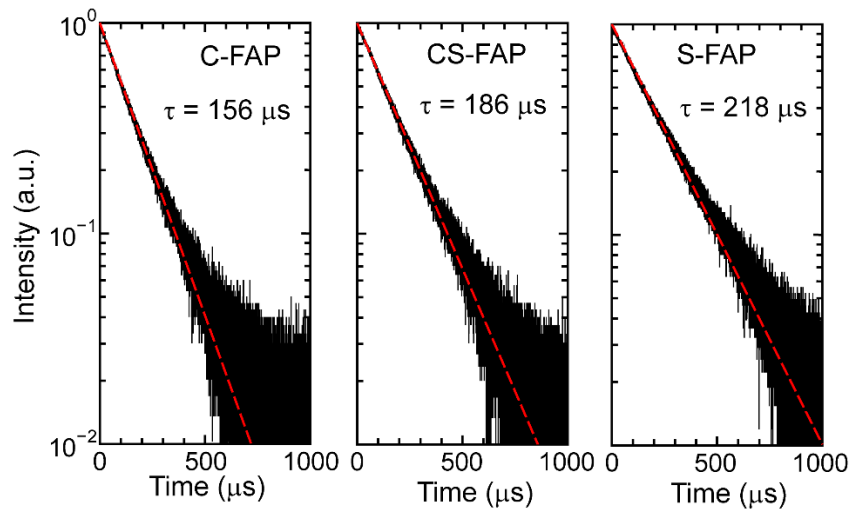


**Fig. 6.** Lifetimes of Nd-doped fluorapatite ceramics.

to the broader emission spectrum, which likely resulted in a lower stimulated emission cross section. At around 1333 nm, laser oscillation was also observed with a slope efficiency of 1.2%. To the best of our knowledge, this is the first demonstration of laser oscillation using Nd:CS-FAP.

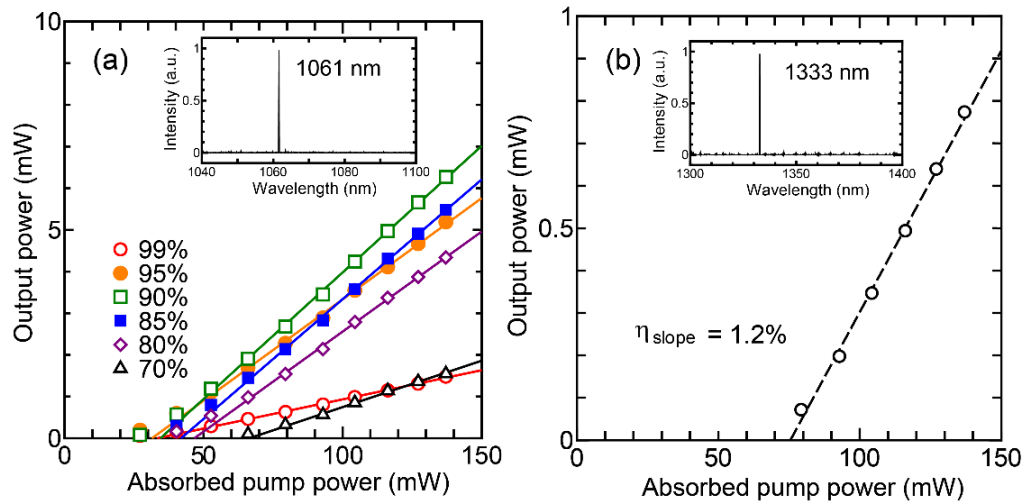


**Fig. 7.** Average output power as a function of the absorbed pump power for Nd:CS-FAP ceramics at (a) 1  $\mu\text{m}$  and (b) 1.3  $\mu\text{m}$  wavelengths. The insets show typical lasing spectra.

Fitting the data for 1  $\mu\text{m}$  yields lasing thresholds of 66.4 mW ( $R = 70\%$ ), 46.7 mW (80%), 41.9 mW (85%), 34.5 mW (90%), 31.4 mW (95%), and 33.3 mW (99%). Although the threshold decreases monotonically up to  $R = 95\%$ , it increases slightly at  $R = 99\%$ . The precise reason for this anomaly remains unclear; however, one possible explanation is that the finite internal loss of the ceramics ( $\sim 0.5 \text{ cm}^{-1}$ ) becomes the dominant loss when the output coupling is extremely low. From the relationship between the output coupler reflectivity (70–95%) and threshold, the cavity loss was estimated to be 19.2%.

Future work will focus on further improving the optical quality of the ceramics through material development. In addition, the introduction of optical coatings and the optimization of crystal thickness and cavity design are planned to enhance laser performance. Additionally, future research will focus on realizing ultrashort pulse operation, thereby advancing this material as a promising candidate for next-generation laser applications.

#### 4. Conclusion

In this study, transparent ceramics of hexagonal mixed fluorapatite Nd:CS-FAP were successfully fabricated, and laser oscillation was demonstrated for the first time. The ceramics exhibited a high optical transmittance of 85.7% for the 0.8 mm thick sample, corresponding to a loss coefficient of  $0.5\text{ cm}^{-1}$ . The ceramics exhibited a hexagonal single-phase with an average grain size of approximately 100 nm. Compared with C-FAP and S-FAP, CS-FAP showed broader absorption and fluorescence spectra, indicating its potential as an ultrashort-pulse laser material. Laser oscillation was observed at both 1061 nm and 1333 nm. Further enhancements in performance can be expected through improvements in the optical quality of the material and optimization of the cavity design.

**Funding.** Japan Science and Technology Agency (JPMJFR203S).

**Acknowledgment.** Portions of this work were presented at Advanced Solid-State Lasers 2025 (ASSL2025), paper JT2uA.16, and has been revised for this manuscript.

**Disclosures.** The authors declare no conflicts of interest.

**Data availability.** Data underlying the results presented in this paper are not publicly available at this time but may be obtained from the authors upon reasonable request.

#### References

1. P. Mason, M. Divoký, K. Ertel, *et al.*, "Kilowatt average power 100 J-level diode pumped solid state laser," *Optica* **4**(4), 438–439 (2017).
2. M. Divoký, J. Pilař, M. Hanuš, *et al.*, "150 J DPSSL operating at 1.5 kW level," *Opt. Lett.* **46**(22), 5771–5773 (2021).
3. T. Sekine, T. Kurita, Y. Hatano, *et al.*, "253 J at 0.2 Hz, LD pumped cryogenic helium gas cooled Yb:YAG ceramics laser," *Opt. Express* **30**(25), 44385–44394 (2022).
4. S. Tokita, M. Divoký, H. Furuse, *et al.*, "Generation of 500-mJ nanosecond pulses from a diode-pumped Yb:YAG TRAM laser amplifier," *Opt. Mater. Express* **4**(10), 2122–2126 (2014).
5. A. Ikesue and Y. L. Aung, "Ceramic laser materials," *Nat. Photonics* **2**(12), 721–727 (2008).
6. R. C. Ohlmann, K. B. Steinbruegge, and R. Mazelsky, "Spectroscopic and laser characteristics of Neodymium-doped calcium fluorophosphate," *Appl. Opt.* **7**(5), 905–914 (1968).
7. X. X. Zhang, G. B. Loutts, M. Bass, *et al.*, "Efficient laser performance of  $\text{Nd}^{3+}:\text{Sr}_5(\text{PO}_4)_3\text{F}$  at 1.059 and 1.328  $\mu\text{m}$ ," *Appl. Phys. Lett.* **64**(24), 3205–3207 (1994).
8. J. B. Gruber, C. A. Morrison, M. D. Seltzer, *et al.*, "Site-selective excitation and polarized absorption spectra of  $\text{Nd}^{3+}$  in  $\text{Sr}_5(\text{PO}_4)_3\text{F}$  and  $\text{Ca}_5(\text{PO}_4)_3\text{F}$ ," *J. Appl. Phys.* **79**(3), 1746–1758 (1996).
9. K. I. Schaffers, J. B. Tassano, A. B. Bayramian, *et al.*, "Growth of Yb: S-FAP [ $\text{Yb}^{3+}:\text{Sr}_5(\text{PO}_4)_3\text{F}$ ] crystals for the Mercury laser," *J. Cryst. Growth* **253**(1–4), 297–306 (2003).
10. A. C. Erlandson, S. M. Aceves, A. J. Bayramian, *et al.*, "Comparison of Nd:phosphate glass, Yb:YAG and Yb:S-FAP laser beamlines for laser inertial fusion energy (LIFE)," *Opt. Mater. Express* **1**(7), 1341–1352 (2011).
11. R. Apetz and M. P. B. Van Bruggen, "Transparent alumina: a light-scattering model," *J. Am. Ceram. Soc.* **86**(3), 480–486 (2003).
12. T. Taira, "Domain-controlled laser ceramics toward Giant Micro-photonics," *Opt. Mater. Express* **1**(5), 1040–1050 (2011).
13. J. Akiyama, Y. Sato, and T. Taira, "Laser demonstration of diode-pumped  $\text{Nd}^{3+}$ -doped fluorapatite anisotropic ceramics," *Appl. Phys. Express* **4**(2), 022703 (2011).
14. Y. Sato, J. Akiyama, and T. Taira, "Process design of microdomains with quantum mechanics for giant pulse lasers," *Sci. Rep.* **7**(1), 10732 (2017).
15. H. Furuse, N. Horiuchi, and B. N. Kim, "Transparent non-cubic laser ceramics with fine microstructure," *Sci. Rep.* **9**(1), 10300 (2019).
16. H. Furuse, T. Okabe, H. Shirato, *et al.*, "High optical-quality non-cubic  $\text{Yb}^{3+}$ -doped  $\text{Ca}_{10}(\text{PO}_4)_6\text{F}_2$  (Yb:FAP) laser ceramics," *Opt. Mater. Express* **11**(6), 1756–1762 (2021).
17. H. Furuse, Y. Mochizuki, D. Kato, *et al.*, "Strontium fluorapatite (S-FAP) nano-grained laser ceramics," *Scr. Mater.* **241**, 115881 (2024).



18. Y. Zhang, Z. Zhou, and B. Mei, "Tunable and enhanced near-infrared luminescence in Nd<sup>3+</sup> doped asymmetrical (Ca<sub>x</sub>Sr<sub>1-x</sub>)<sub>5</sub>(PO<sub>4</sub>)<sub>3</sub>F transparent ceramic," *J. Eur. Ceram. Soc.* **44**(10), 5744–5751 (2024).
19. C. Kränkel, A. Uvarova, C. Gugushev, *et al.*, "Rare-earth doped mixed sesquioxides for ultrafast lasers," *Opt. Mater. Express* **12**(3), 1074–1091 (2022).
20. T. T. Basiev, N. A. Es'kov, A. Y. Karasik, *et al.*, "Disordered garnets Ca<sub>3</sub>(Nb, Ga)<sub>5</sub>O<sub>12</sub>:Nd<sup>3+</sup>—prospective crystals for powerful ultrashort-pulse generation," *Opt. Lett.* **17**(3), 201–203 (1992).
21. J. Saikawa, Y. Sato, T. Taira, *et al.*, "Absorption, emission spectrum properties, and efficient laser performances of Yb:Y<sub>3</sub>ScAl<sub>4</sub>O<sub>12</sub> ceramics," *Appl. Phys. Lett.* **85**(11), 1898–1900 (2004).
22. W. Jing, P. Loiko, J. M. Serres, *et al.*, "Synthesis, spectroscopy, and efficient laser operation of "mixed" sesquioxide Tm:(Lu,Sc)<sub>2</sub>O<sub>3</sub> transparent ceramics," *Opt. Mater. Express* **7**(11), 4192–4202 (2017).
23. S. A. Payne, L. D. DeLoach, L. K. Smith, *et al.*, "Ytterbium-doped apatite-structure crystals: A new class of laser materials," *J. Appl. Phys.* **76**(1), 497–503 (1994).
24. X. Long, Y. P. Tong, P. M. W. French, *et al.*, "Multi-siting and mode locking in a Yb<sup>3+</sup>:CS-FAP laser," *Opt. Commun.* **141**(3–4), 162–166 (1997).
25. K. Takimoto, H. Sone, and H. Furuse, "Laser properties of Nd:FAP and Nd:S-FAP ceramics at 1.06 and 1.33μm," *Jpn. J. Appl. Phys.* **64**(6), 060905 (2025).
26. P. Becker, E. Libowitzky, R. Kleinschrodt, *et al.*, "Linear optical properties and raman spectroscopy of natural fluorapatite," *Cryst. Res. Technol.* **51**(4), 282–289 (2016).